Modular modelling of combined AC and DC systems in dynamic simulations

Petros Aristidou
Lampros Papangelis
Dept. of Elec. Eng. and Comp. Science,
University of Liège, Belgium
{p.aristidou, l.papangelis}@ulg.ac.be

Xavier Guillaud
L2EP - Ecole Centrale de Lille,
France
xavier.guillaud@ec-lille.fr

Thierry Van Cutsem
Fund for Scientific Research (FNRS) at
Dept. of Elec. Eng. and Comp. Science,
University of Liège, Belgium
t.vancutsem@ulg.ac.be

Abstract—A formulation is proposed in which an AC-DC system is modeled as a combination of AC grids, DC grids, injectors, AC two-ports and AC/DC converters, respectively. This modular modelling facilitates the dynamic simulation of future complex AC/DC systems. Furthermore, it can be exploited by the solver, which performs less operations on components with lower dynamic activity, and offers parallel processing of the time simulation. This approach is illustrated on a test system in which a multi-terminal DC grid connects two asynchronous AC systems, allows frequency support between them, and acts as emergency control against AC voltage instability.

Index Terms—Time simulation, phasor approximation, AC/DC systems, multi-terminal DC system, domain decomposition methods, Schur complement, parallel processing.

Figure 1: Illustrative example of combined AC-DC system

I. Introduction

The increasing opening of electricity markets, the decommissioning of traditional power plants, and the harvesting of sustainable energy from remote (in particular off-shore) locations will result in larger power transfers over longer distances. This imperative evolution of transmission grids, as well as the progress made in Voltage Source Converters (VSCs), has triggered a vibrant development of High-Voltage Direct Current (HVDC) systems [1], [2]. As a result, more and more HVDC interconnections are in operation or planned.

While point-to-point links have become very common [2], Multi-Terminal DC (MTDC) systems are the next step envisaged [3], [4]. They will result in more complex HVDC network topologies. An illustrative example is sketched in Fig. 1 where AC grids are shown with gray boxes, and DC with white. The system includes two point-to-point HVDC links. One of them allows power exchange (and possibly frequency support) between the asynchronous AC systems #1 and #2. The other link connects a wind park to AC system #2. The overlay MTDC grid #1 serves as a backbone reinforcing AC system #1 by offering an alternative path for power transfers between remote locations inside that system. The MTDC grid #2 collects the energy produced by two off-shore wind parks but also allows power transfers between the AC systems #1 and #2. The generators within each wind park are connected through AC cables which make up a separate AC grid. The latter can be modeled in detail or replaced by a single, isolated AC bus if the generators are lumped into one equivalent.
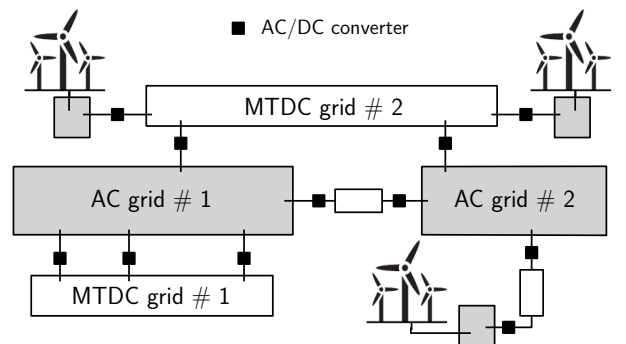
In the future, the need for dynamic simulation of combined AC and DC systems will keep increasing [5]. For instance, HVDC systems are expected to take a greater part in frequency and voltage control [6]. Furthermore, the response of AC/DC converters to nearby faults in AC grids must be taken into account when assessing system security.

To reproduce the dynamics of AC/DC converters, Electro-Magnetic Transient (EMT) simulation remains the reference in terms of accuracy. However, the EMT models are not suited to the large-scale studies and long-term dynamics considered in this paper, for which the phasor approximation is preferred.

To anticipate the future developments, while accommodating the above mentioned diversity of HVDC system topologies, there is a need for a flexible AC-DC system dynamic modelling. Models of point-to-point HVDC links have been available for quite some time in industry-grade dynamic simulation software [7]. While their developers certainly work towards incorporating MTDC systems, there are, to the authors' knowledge, few publications devoted to such developments.

This paper proposes a modular formulation making it easy to develop, extend and maintain models for an MTDC topology of arbitrary complexity.

Furthermore, the modular modelling can be exploited by the dynamic simulation solver. In this respect, a Schur-complement-based formulation is described in this paper, which allows the individual components to be processed separately during the simulation. This makes it possible, for instance, to update Jacobians locally and to perform less New-

ton iterations on components with lower participation in the dynamic response. It also paves the way to parallel processing of the computations to further accelerate the simulations.

These features are present in RAMSES, a research software developed at the University of Liège [8], whose results are presented in this paper.

II. MODULAR MODELLING OF AN AC-DC SYSTEM

A. AC and DC transmission sub-networks

Modular modeling is built upon the concept of the transmission grid being an arbitrary combination of (disjoint) AC and DC sub-networks. In the case of Fig. 1, for instance, the transmission grid can be considered to include five AC and four DC sub-networks.

Under the phasor approximation, AC networks are represented by the well-known algebraic equations:

$$\underbrace{\begin{bmatrix} \boldsymbol{G} & -\boldsymbol{B} \\ \boldsymbol{B} & \boldsymbol{G} \end{bmatrix}}_{\boldsymbol{D}} \underbrace{\begin{bmatrix} \boldsymbol{v}_x \\ \boldsymbol{v}_y \end{bmatrix}}_{\boldsymbol{v}_{ac}} - \begin{bmatrix} \boldsymbol{i}_x \\ \boldsymbol{i}_y \end{bmatrix} = \boldsymbol{0} \qquad (1)$$

where $\boldsymbol{G}$ (resp. $\boldsymbol{B}$) is the nodal conductance (resp. susceptance) matrix, $\boldsymbol{v}_x$ and $\boldsymbol{v}_y$ are vectors of real and imaginary components of the bus voltage, and $\boldsymbol{i}_x$ and $\boldsymbol{i}_y$ are the corresponding injected current components.

Similarly, by neglecting the series inductances of DC lines and cables, and accounting for their shunt capacitances in the AC/DC converters [9], the DC grid is represented by a network of resistances, modelled by:

$$\boldsymbol{G}_{dc}\boldsymbol{v}_{dc} - \boldsymbol{i}_{dc} = \boldsymbol{0} \qquad (2)$$

where $\boldsymbol{G}_{dc}$ the nodal conductance matrix, $\boldsymbol{v}_{dc}$ is the vector of DC bus voltages, and $\boldsymbol{i}_{dc}$ the vector of injected DC currents.

This encompasses any AC-DC grid topology. If there are several disjoint AC sub-networks, the $\boldsymbol{G}$ and $\boldsymbol{B}$ matrices have a block-diagonal structure. The same holds true for $\boldsymbol{G}_{dc}$ in case of disjoint DC sub-networks. In the system of Fig. 1, for instance, $\boldsymbol{G}$ and $\boldsymbol{B}$ have five nonzero diagonal blocks, while $\boldsymbol{G}_{dc}$ has four such blocks.

B. Equipment connected to AC or DC grids

Modularity is also obtained by matching any equipment connected to the AC or DC grids with one of the following three generic components:

- an *injector* connected to a single AC bus
- an *AC two-port* connecting two AC buses
- an *AC/DC converter* connecting one AC and one DC bus.

Each component is modelled by a system of Differential-Algebraic Equations (DAEs). Including algebraic equations and states offers remarkable modelling flexibility. In particular, each component model interfaces with the network through the currents injected into it, involved in the DAEs as algebraic states. This allows processing the components separately during the simulation, as mentioned in the Introduction.

Each of the above three generic components is considered hereafter in some more detail, with reference to Fig. 2.
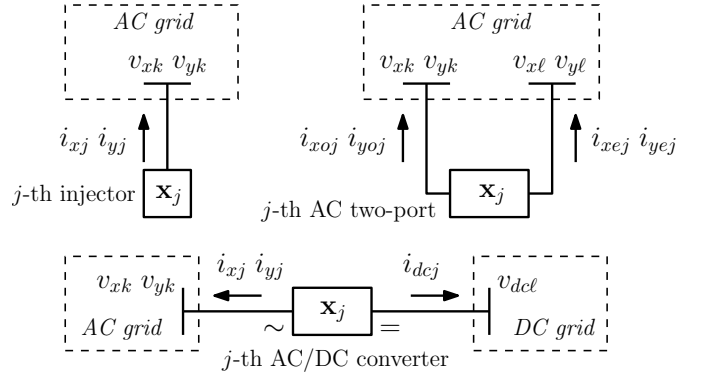

Figure 2: The three generic components

C. Injector

Synchronous machines, synchronous condensers, static var compensators, motors, static loads, wind-turbine generators, etc. are well-known examples of injectors. The j-th injector attached to the k-th AC bus is modelled by:

$$\boldsymbol{\Gamma}_j\dot{\boldsymbol{x}}_j = \boldsymbol{\Phi}_j(\boldsymbol{x}_j, v_{xk}, v_{yk}) \qquad (3)$$

where $\boldsymbol{x}_j$ is a state vector including both differential and algebraic variables, v_{xk} and v_{yk} are the bus voltage components. In this and subsequent models, $\boldsymbol{\Gamma}_j$ is a diagonal matrix with $(\boldsymbol{\Gamma}_j)_{\ell\ell} = 0$ if the ℓ-th equation is algebraic, and one otherwise. The use of $\boldsymbol{\Gamma}_j$ provides additional modelling flexibility to handle nonlinearities by changing a differential equation into an algebraic one during the simulation, and conversely [10]. Formally this corresponds to changing a diagonal entry of $\boldsymbol{\Gamma}_j$ from one to zero, and conversely. This feature is available in the solver of RAMSES.

Note that $\boldsymbol{x}_j$ includes in particular the components of the current injected in the connection bus, i.e. $\boldsymbol{x}_j = [i_{xj}\ i_{yj}\ \ldots]^T$.

D. AC two-port

While an injector is attached to a single AC bus, an AC two-port is aimed at connecting two AC buses. Thus, the generic model of j-th AC two-port connected to the k-th and l-th AC buses is:

$$\boldsymbol{\Gamma}_j\dot{\boldsymbol{x}}_j = \boldsymbol{\Phi}_j(\boldsymbol{x}_j, v_{xk}, v_{yk}, v_{xl}, v_{yl}) \qquad (4)$$

$\boldsymbol{x}_j$ includes the components of the currents injected in both AC buses, i.e. $\boldsymbol{x}_j = [i_{xoj}\ i_{yoj}\ i_{xej}\ i_{yej}\ \ldots]^T$ where subscript o denotes the origin and e the extremity.

E. AC/DC converter

An AC/DC converter connects one AC with one DC bus. Thus, the j-th AC/DC converter connecting the k-th AC bus and the l-th DC bus is modelled by:

$$\boldsymbol{\Gamma}_j\dot{\boldsymbol{x}}_j = \boldsymbol{\Phi}_j(\boldsymbol{x}_j, v_{xk}, v_{yk}, v_{dcl}) \qquad (5)$$

where v_{dcl} is the DC bus voltage. $\boldsymbol{x}_j$ includes the current components: $\boldsymbol{x}_j = [i_{xj}\ i_{yj}\ i_{dcj}\ \ldots]^T$.

Note that a point-to-point DC link can be modelled either as an AC two-port, or as the combination of two AC/DC converters and one DC line. In the latter case (sketched in Fig. 1), a separate DC sub-network with two buses is created.

III. Solution Algorithm

Let the AC network equations (1) be rewritten as:

$$0 = \boldsymbol{D}\boldsymbol{v}_{ac} - \sum_{j=1}^{N} \boldsymbol{C}_j \boldsymbol{x}_j \triangleq \boldsymbol{g}_{ac}(\boldsymbol{x}, \boldsymbol{v}_{ac}) \qquad (6)$$

where N is the total number of injectors, AC two-ports and AC/DC converters in the system. $\boldsymbol{C}_j$ is a matrix with zeros and ones whose purpose is to extract the AC current components from the various $\boldsymbol{x}_j$ state vectors and add them to the proper network equations.

Similarly, the DC network equations (2) are rewritten as:

$$0 = \boldsymbol{G}_{dc}\boldsymbol{v}_{dc} - \sum_{j=1}^{N_{dc}} \boldsymbol{E}_j \boldsymbol{x}_j \triangleq \boldsymbol{g}_{dc}(\boldsymbol{x}, \boldsymbol{v}_{dc}) \qquad (7)$$

where N_{dc} is the number AC/DC converters, and $\boldsymbol{E}_j$ is also a matrix with zeros and ones.

For the purpose of numerical simulation, the DAE systems (3), (4) and (5) are algebraized using a differentiation formula, such as Trapezoidal Rule or Backward Differentiation Formula (BDF). This yields the algebraized equations in compact form:

$$0 = \boldsymbol{f}_j(\boldsymbol{x}_j, \boldsymbol{v}_{ac}, \boldsymbol{v}_{dc}), \quad j = 1, \ldots, N. \qquad (8)$$

At each discrete time t_m the nonlinear equations (8) are solved together with the AC-DC network equations (6, 7) using a Newton method to obtain the vectors $\boldsymbol{x}_j(t_m)$, $\boldsymbol{v}_{ac}(t_m)$ and $\boldsymbol{v}_{dc}(t_m)$. At the k-th Newton iteration, the following linear equations have to be solved ($j = 1, \ldots, N$):

$$\boldsymbol{A}_j \Delta \boldsymbol{x}_j^k + \begin{bmatrix} \boldsymbol{B}_j & \boldsymbol{H}_j \end{bmatrix} \begin{bmatrix} \Delta \boldsymbol{v}_{ac}^k \\ \Delta \boldsymbol{v}_{dc}^k \end{bmatrix} = -\boldsymbol{f}_j(\boldsymbol{x}_j^{k-1}, \boldsymbol{v}_{ac}^{k-1}, \boldsymbol{v}_{dc}^{k-1}) \quad (9)$$

$$\boldsymbol{D}\Delta \boldsymbol{v}_{ac}^k - \sum_{j=1}^{N} \boldsymbol{C}_j \Delta \boldsymbol{x}_j^k = -\boldsymbol{g}_{ac}(\boldsymbol{x}^{k-1}, \boldsymbol{v}_{ac}^{k-1}, \boldsymbol{v}_{dc}^{k-1}) \quad (10)$$

$$\boldsymbol{G}_{dc}\Delta \boldsymbol{v}_{dc}^k - \sum_{j=1}^{N_{dc}} \boldsymbol{E}_j \Delta \boldsymbol{x}_j^k = -\boldsymbol{g}_{dc}(\boldsymbol{x}^{k-1}, \boldsymbol{v}_{ac}^{k-1}, \boldsymbol{v}_{dc}^{k-1}) \quad (11)$$

where Δ denotes a vector correction, $\boldsymbol{A}_j$ is the Jacobian of the j-th component towards its state variables $\boldsymbol{x}_j$, $\boldsymbol{B}_j$ towards $\boldsymbol{v}_{ac}$ and $\boldsymbol{H}_j$ towards $\boldsymbol{v}_{dc}$.

The above equations are solved in a decomposed way by reorganizing them as follows. The injector, the AC two-port and the AC/DC converter state vector corrections $\Delta \boldsymbol{x}_j^k$ are obtained from Eqs. (9) and introduced in Eqs. (10) and (11), to obtain the Schur-complement system of Eq. (12) (see next page). Then, at each Newton iteration, the latter system is solved to obtain the voltage corrections $\Delta \boldsymbol{v}_{ac}^k$ and $\Delta \boldsymbol{v}_{dc}^k$ which are substituted in the various sets of equations (9). The latter are then solved to obtain the state corrections $\Delta \boldsymbol{x}_j^k$.

This procedure removes the data dependencies between the various components, allowing their respective sets of equations to be solved independently. In fact, both the modular modelling and the Schur-complement formulation allow many calculations associated with injectors, AC two-ports or AC/DC converters to be performed independently of each other: DAE
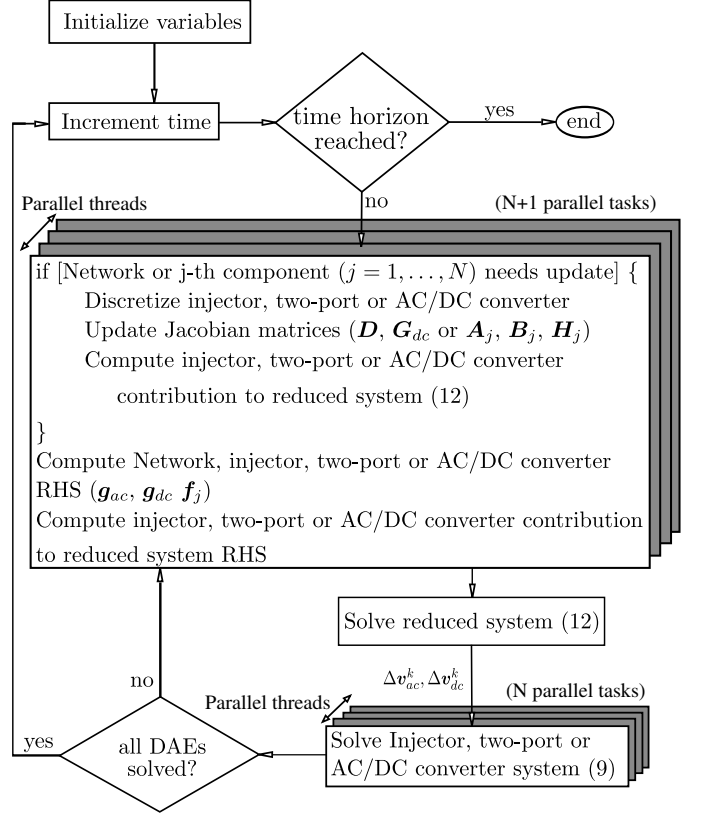

Figure 3: Decomposed and parallelized simulation algorithm

system discretization, Jacobian and Schur-complement computation, matrix factorization, linear system solution, etc. Thus, shared-memory parallel computing techniques are employed to accelerate the dynamic simulation as shown in Fig. 3.

As is well-known, the $\boldsymbol{D}$ and $\boldsymbol{G}_{dc}$ matrices have a very sparse structure, inherited from the sparse nodal admittance matrix. As explained hereafter, sparsity is very little affected by the elimination of the $\Delta \boldsymbol{x}_j^k$ variables. Hence, the Schur-complement matrix in the left hand side of Eq. (12) is also very sparse, allowing fast network solutions.

It has to be noted first that $\boldsymbol{B}_j$ and $\boldsymbol{H}_j$ are extremely sparse matrices. For an injector, since the model involves only two AC voltage components (v_{xk}, v_{yk}), only two columns of $\boldsymbol{B}_j$ are non-zero, corresponding to the positions of v_{xk} and v_{yk} in $\boldsymbol{v}_{ac}$. Similarly, for an AC two-port, $\boldsymbol{B}_j$ includes four non-zero columns while, for an AC/DC converter, $\boldsymbol{B}_j$ includes two non-zero columns and $\boldsymbol{H}_j$ one.

From the sparsity patterns of matrices $\boldsymbol{C}_j$ and $\boldsymbol{B}_j$, it can be shown that the $\boldsymbol{C}_j \boldsymbol{A}_j^{-1} \boldsymbol{B}_j$ contribution of an injector has only four non-zero elements which modify four, already non-zero, elements of $\boldsymbol{D}$, corresponding to v_{xk} and v_{yk}. Those elements are shown with squares in Fig. 4.

Similarly, the $\boldsymbol{C}_j \boldsymbol{A}_j^{-1} \boldsymbol{B}_j$ contribution of an AC two-port consists of sixteen nonzero elements. Eight of them modify already nonzero entries of a diagonal sub-matrix of $\boldsymbol{D}$, corresponding to v_{xk}, v_{yk}, v_{xl} and v_{yl}. The other eight, off-diagonal terms correspond to couplings between these variables.

$$\left(\begin{bmatrix} \boldsymbol{D} & \boldsymbol{0} \\ \boldsymbol{0} & \boldsymbol{G}_{dc} \end{bmatrix} + \begin{bmatrix} \sum_j^N \boldsymbol{C}_j \boldsymbol{A}_j^{-1} \begin{bmatrix} \boldsymbol{B}_j & \boldsymbol{H}_j \end{bmatrix} \\ \sum_j^{N_{dc}} \boldsymbol{E}_j \boldsymbol{A}_j^{-1} \begin{bmatrix} \boldsymbol{B}_j & \boldsymbol{H}_j \end{bmatrix} \end{bmatrix} \right) \begin{bmatrix} \Delta\boldsymbol{v}_{ac} \\ \Delta\boldsymbol{v}_{dc} \end{bmatrix} = \begin{bmatrix} -\boldsymbol{g}_{ac}(\boldsymbol{x}^{k-1}, \boldsymbol{v}_{ac}^{k-1}, \boldsymbol{v}_{dc}^{k-1}) - \sum_j^N \boldsymbol{C}_j \boldsymbol{A}_j^{-1} \boldsymbol{f}_j(\boldsymbol{x}_j^{k-1}, \boldsymbol{v}_{ac}^{k-1}, \boldsymbol{v}_{dc}^{k-1}) \\ -\boldsymbol{g}_{dc}(\boldsymbol{x}^{k-1}, \boldsymbol{v}_{ac}^{k-1}, \boldsymbol{v}_{dc}^{k-1}) - \sum_j^{N_{dc}} \boldsymbol{E}_j \boldsymbol{A}_j^{-1} \boldsymbol{f}_j(\boldsymbol{x}_j^{k-1}, \boldsymbol{v}_{ac}^{k-1}, \boldsymbol{v}_{dc}^{k-1}) \end{bmatrix} \quad (12)$$
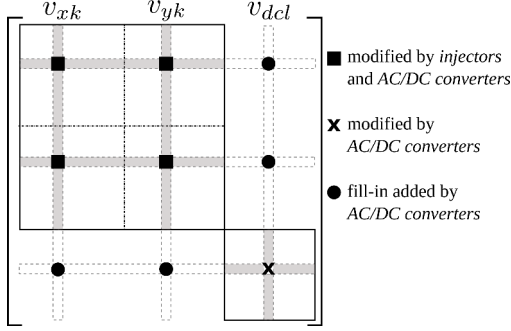

Figure 4: Contribution of injectors and AC/DC converters to the Schur-complement matrix in the left-hand side of Eq. (12)

Figure 5: Overall structure of the test system

Finally, the $\boldsymbol{C}_j \boldsymbol{A}_j^{-1} \boldsymbol{B}_j$, $\boldsymbol{C}_j \boldsymbol{A}_j^{-1} \boldsymbol{H}_j$, $\boldsymbol{E}_j \boldsymbol{A}_j^{-1} \boldsymbol{B}_j$ and $\boldsymbol{E}_j \boldsymbol{A}_j^{-1} \boldsymbol{H}_j$ matrices of an AC/DC converter contribute with nine nonzero elements. They modify four, already nonzero, elements of $\boldsymbol{D}$ corresponding to v_{xk}, v_{yk} as well as one element of $\boldsymbol{G}_{dc}$ corresponding to v_{dcl}. Those five terms are shown with squares and cross in Fig. 4. The remaining four contributions correspond to couplings between these variables; they are shown with disks in Fig. 4.

Obviously, sparse matrix storage is used for $\boldsymbol{D}$, $\boldsymbol{G}_{dc}$, $\boldsymbol{B}_j$, $\boldsymbol{E}_j$, $\boldsymbol{C}_j$ and $\boldsymbol{H}_j$ whose sparsity patterns are known beforehand from the network topology. Only the nonzero elements of each correction term are computed, by solving linear systems with coefficient matrices $\boldsymbol{A}_j$.

Last but not least, the Jacobian matrices are updated infrequently and kept constant over several Newton iterations or even discrete time steps. They are updated only if convergence has not taken place after a number of Newton iterations at the same discrete time-step.

IV. SIMULATION RESULTS

A. Test system

The system shown in Figs. 5 and 6 was modeled as described in Section II and simulated with the algorithms of Section III. It consists of two asynchronous AC systems and one offshore wind farm, connected through a five-terminal HVDC grid equipped with five VSCs.

The "East" AC system is based on the so-called Nordic test system. The starting point was the variant documented in [11], at its insecure operating point A. With respect to [11], the system was modified as follows:

- the large, equivalent generator connected to bus 4072 was removed and replaced by the T1E converter;
- another connection to the DC grid was added at bus 4051, through the T2E converter. This allows using the MTDC system as an overlay grid reinforcing the AC system.
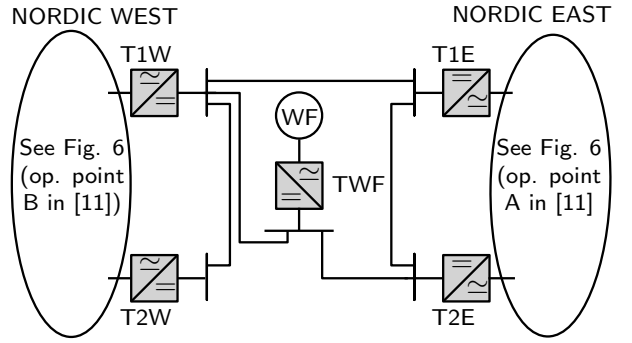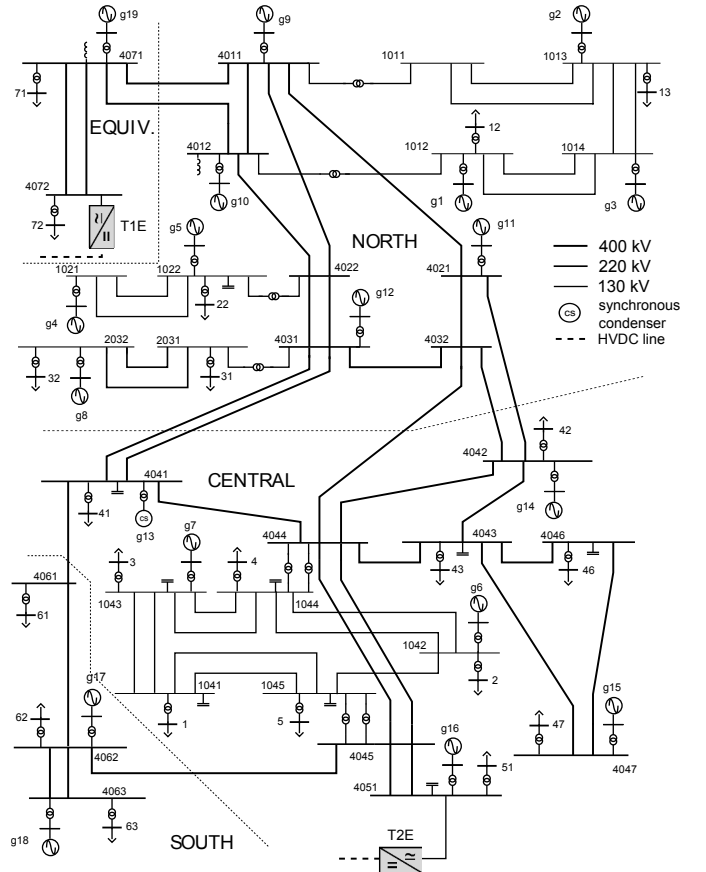

Figure 6: Nordic test system with HVDC grid connections

The modified system is shown in Fig. 6. It includes 73 buses and 19 synchronous machines modeled in detail with their regulators. The voltage-dependent loads are represented behind distribution transformers equipped with Load Tap Changers (LTCs) reacting with various delays.

The "Nordic West" system is a mirror copy of its East counterpart, but operating at the secure point B documented in [11]. It is connected to the DC grid through T1W and T2W.

The Wind Farm is modeled through a simple two-bus AC grid connected through the TWF converter (see Fig. 5).

The modelling of Section II yields a 5×5 matrix $\mathbf{G}_{dc}$, while matrices $\mathbf{G}$ and $\mathbf{B}$ have three nonzero diagonal blocks corresponding to the East, West and WF grids, respectively.

The five AC/DC converters, of the VSC type, are modeled in detail, as recommended in [3], [9], [12]. The TWF converter imposes constant voltage and frequency on the AC side, thus acting as a slack bus. The other four converters operate in voltage-droop mode. Thus, when the wind farm output changes, the current collected by TWF varies and the resulting power change is shared by T1E, T2E, T1W and T2W.

Last but not least, these four VSCs are provided each with the frequency support control proposed in [13]. Then the controller uses the local frequency measurement f as input, and outputs a correction which is added to the active power set-point of the VSC, together with the voltage droop term. The control becomes active when frequency leaves a predefined deadband. Then, through integral control, the active power P in the VSC is forced to follow in steady-state a $P - f$ droop characteristic, similar to the speed droop characteristic of a conventional speed governor.

B. Scenario and system response

The example reported here involves frequency support between AC systems, as well as an emergency control with the HVDC grid stabilizing the AC system in the long term. The initial event is the outage of generator g17 in the East system.

This disturbance causes the frequency drop shown in Fig. 7. Without frequency support, the East frequency drops by 350 mHz, while the West frequency remains unaffected. With frequency support, the controllers present in T1E and T2E activate the help of the East system by the West one by actuating a power transfer through the HVDC grid. This is triggered when frequency drops by more than 200 mHz, which is sensed by the T2E converter at $t = 1.2$ s and by T1E at $t = 1.4$ s. The benefit of this control is to reduce the frequency drop in the East system to 300 mHz, while the West system frequency undergoes a moderate variation, as shown in Fig. 7.

At $t = 100$ s, the frequency support control is automatically deactivated when the East frequency has recovered [13].

The system recovers but, in the long term, under the effect of LTCs attempting to restore distribution voltages and OverExcitation Limiters (OELs) bringing generator field currents below their limits, voltage instability takes place and the system eventually collapses at $t \simeq 120$ s, as shown in Fig. 8. This instability results from the increased power transfer in the lines between the North and Central areas (see Fig. 6) when the production lost in the Central area is compensated by the generators in the North [11]. With the frequency support control, the power injected by T2E somewhat relieves those lines and yields a slightly better, but still unstable voltage evolution, as shown by the dashed curve in Fig. 8.
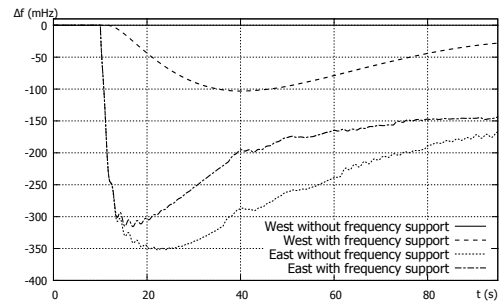

Figure 7: Frequency deviations in East and West systems

To relieve those lines, a remedial action consists of transferring power from North to Central areas through the HVDC grid. To this purpose, from $t = 120$ to 140 s, the active power set-point of T1E is ramped down by 200 MW while that of T2E is ramped up by the same amount. The resulting voltage stabilization is easily seen from Fig. 8.

The evolution of VSC active powers and DC voltages including both remedial actions, are shown in Figs. 9 and 10, respectively. During the frequency support period, DC voltages drop due to the power request that draws on the energy stored in the DC capacitors. This is promptly compensated by the VSC controls, and the DC voltages settle to values dictated by the voltage droop settings of T1W and T2W. By properly tuning the frequency support controller, the overshoot in the active power response of T1E and T2E, and the DC voltage depletion are very limited [13]. The power ramping of T1E and T2E to stabilize voltages in the long term is easily seen in Fig. 9. The power changes in T1W and T2W are negligible, and the power transfer from West to East remains unchanged.

V. Profiling the modular solver performance

Table I lists the major operations performed during the whole simulation until the system returns to steady state. The step size used is 20 ms. It also shows which of them are performed in parallel and the percentage of the execution time in the parallel or sequential sections, respectively. The remaining time is spent on handling the time-step initialization, bookkeeping, output of computed values, etc.

It can be seen that the time spent to update, factorize and solve the reduced system (12) is small compared to the overall simulation time. This is due to the infrequent update of the Schur-complement matrix (only 18 times throughout the simulation) and to the sparsity of the matrix which allows employing fast, sparse linear solvers. The largest percentage of the simulation time is spent on updating, factorizing and solving the injector and AC/DC converter systems (9). Figure 11 shows the total number of solutions performed at every time step. It can be seen that the number of solutions spikes after major events (generator tripping, OEL action, activation of controls, etc.).

However, since these operations can be performed in parallel, the simulation time decreases when using a standard multicore machine. For instance, using a quad-core laptop with i7-4710MQ CPU @ 2.50GHz and 16GB RAM, the sequential
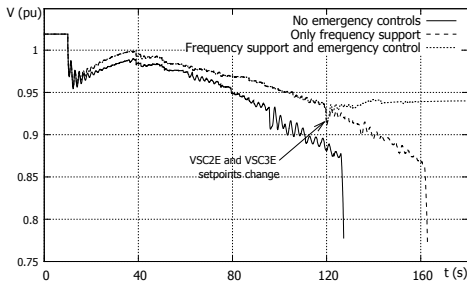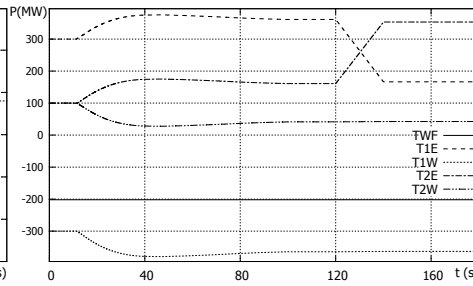
Figure 8: Voltage at bus 1041
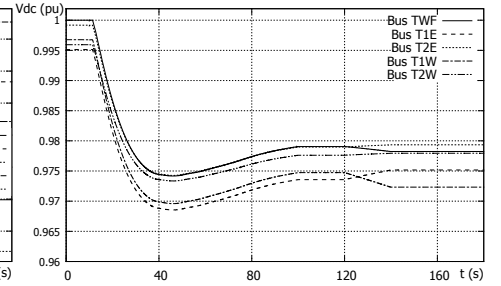

Figure 9: Active power of VSCs

Figure 10: DC voltages

Table I: Major operations over the entire simulation

| Type of operation	Nb	Parallel	%
Update and factorize the Schur-complement matrix in (13)	18	No	8
Solve reduced system (13)	18127	No	
Evaluate g_{dc} and g_{ac}	40948	No	
Update and factorize injector matrices and Schur-complement factors	408361	Yes	60
Update and factorize AC/DC converter matrices and Schur-complement factors	457	Yes	
Solve injector system (10)	1415630	Yes	
Solve AC/DC converter system (10)	79972	Yes	
Evaluate injector functions f_j	4938315	Yes	
Evaluate AC/DC Converter RHS f_j	284712	Yes	
Remaining operations	-	No	32
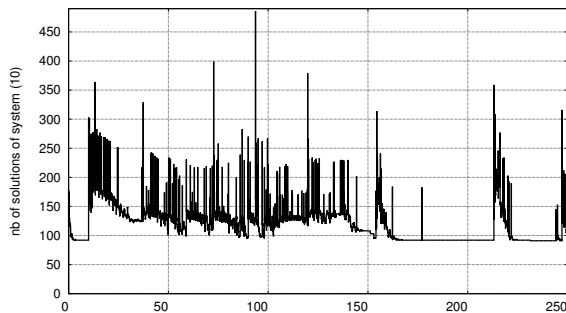
Figure 11: Number of systems (9) relative to injectors and AC/DC converters solved at each time step

execution takes 5.2 s, while a simulation in parallel using the four cores takes 3.7 s. That is, the simulation is 1.41 times faster, even on this small test system, and using a standard computer. Overall, as 60% of the operations are performed in parallel, and by ignoring any parallelization overhead and imbalances, the computation can be *up to* 2.5 times faster compared to a sequential run of the same algorithm.

It is noteworthy that even the sequential execution of the algorithm is very fast as it takes advantage of the modularity to update and compute the injectors and the AC/DC converters asynchronously, only when needed.

VI. Conclusion

A modular modelling has been proposed allowing to handle AC and DC network topologies of virtually any complexity. To this purpose, the system is seen as a combination of AC grids, DC grids, injectors, AC two-ports and AC/DC converters,

respectively.

This modularity is exploited by the solver, which performs less operations on components with lower dynamic activity, and offers parallel processing of the time simulation. This is made possible by a Schur-complement-based decomposition allowing to solve the equations of the above mentioned components separately, with asynchronous update of Jacobians. The sparsity of the involved matrices is exploited extensively.

The approach has been illustrated on a test system in which a multi-terminal DC grid allows frequency support between asynchronous AC grids, and provides emergency control against AC voltage instability. In spite of the small system size, the results confirm the advantages of the proposed modelling and computational procedure.

References

[1] "Ten year network development plan 2010-2020," tech. rep., ENTSO-E, 2010.

[2] CIGRE Tech. Brochure JWG C4/B4/C1.604, *Influence of Embedded HVDC Transmission on System Security and AC Network Performance*, 2013.

[3] P. Rault, X. Guillaud, F. Colas, and S. Nguefeu, "Method for small signal stability analysis of VSC-MTDC grids," in *Proc. of IEEE PES General Meeting*, 2012.

[4] D. Van Hertem and M. Ghandhari, "Multi-terminal VSC HVDC for the European supergrid: Obstacles," *Renewable and Sustainable Energy Reviews*, vol. 14, no. 9, pp. 3156–3163, 2010.

[5] J. Beerten, O. Gomis-Bellmunt, X. Guillaud, J. Rimez, A. van der Meer, and D. Van Hertem, "Modeling and control of hvdc grids: A key challenge for the future power system," in *Proc. of PSCC*, 2014.

[6] "Entso-e draft network code on high voltage direct current connections and dc connected power park modules," 2014.

[7] S. Cole and B. Haut, "Robust modeling against model-solver interactions for high-fidelity simulation of VSC HVDC systems in EUROSTAG," *IEEE Trans. on Power Systems*, vol. 28, no. 3, pp. 2632–2638, 2013.

[8] P. Aristidou, D. Fabozzi, and T. Van Cutsem, "Dynamic simulation of large-scale power systems using a parallel Schur-complement-based decomposition method," *IEEE Trans. on Parallel and Distributed Systems*, vol. 25, no. 10, pp. 2561–2570, 2014.

[9] S. Cole and R. Belmans, "A proposal for standard VSC HVDC dynamic models in power system stability studies," *Electric Power Systems Research*, vol. 81, no. 4, pp. 967–973, 2011.

[10] D. Fabozzi, A. S. Chieh, P. Panciatici, and T. Van Cutsem, "On simplified handling of state events in time-domain simulation," in *Proc. of PSCC*, 2011.

[11] T. Van Cutsem and L. Papangelis, "Description, modeling and simulation results of a test system for voltage stability analysis," internal report, University of Liège, 2013. http://hdl.handle.net/2268/141234.

[12] M. Imhof and G. Andersson, "Dynamic modeling of a VSC-HVDC converter," in *Proc. Universities Power Engineering Conference*, 2013.

[13] L. Papangelis, X. Guillaud, and T. Van Cutsem, "Frequency support among asynchronous AC systems through VSCs emulating power plants," in *11th IET Conf. on AC and DC Power Transmission*, 2015.